



A testcase for the inviscid shallow water equations on the sphere

R. K. Scott^{*a} & L. M. Harris^b & L. M. Polvani^c

^a*School of Mathematics and Statistics, University of St Andrews, St Andrews, UK*

^b*NOAA/Geophysical Fluid Dynamics Laboratory, Princeton University, Princeton, New Jersey, USA*

^c*Dept of Applied Physics and Applied Mathematics, and Dept of Earth and Environmental Sciences, Columbia University, New York, USA*

*Correspondence to: R. K. Scott, School of Mathematics and Statistics, University of St Andrews, St Andrews, KY16 9SS, UK

A numerically converged solution to the inviscid global shallow water equations on a predefined time interval is documented to provide a convenient benchmark for model validation. The solution is based on the same initial conditions as a previously documented solution for the viscous equations. The solution is computed using two independent numerical schemes, one a pseudospectral scheme based on an expansion in spherical harmonics, the other a finite-volume scheme on a cubed-sphere grid. Flow fields and various integral norms are both documented to facilitate model comparison and validation. Attention is drawn to the utility of the potential vorticity supremum as a convenient and sensitive test of numerical convergence, in which the exact value is known *a priori* over the entire time interval. Copyright © 2013 Royal Meteorological Society

Key Words:

Received ...

Citation: ...

1. Introduction

The development of accurate and efficient numerical schemes for solving the equations of motion that govern fundamental atmospheric dynamics underpins our capability for accurate numerical weather forecasting and climate prediction. Such development is a hierarchical process, involving many stages from theoretical numerical analysis to the implementation of general circulation models on specific computer architectures. Once a particular numerical scheme has been implemented, the next important stage of the development process involves the testing and validation of the scheme against known solutions of the equations of motion. This stage has two distinct objectives: at the first level, the objective is to ensure that the numerical scheme can be integrated stably and converges to the correct solution; thereafter it is desirable to assess the accuracy and efficiency of the scheme against alternatives. To the extent to which it is possible, such tests should be carried out using solutions that are representative of the actual flows encountered in the atmosphere, flows that typically involve strong nonlinearity, chaotic time evolution, and the rapid generation of small scales, [in particular fronts and other](#) strong gradients in the dynamical variables.

[An important aspect of any atmospheric general circulation model is the formulation of the horizontal discretization, in particular the nonlinear horizontal advection. This may frequently be considered independently of vertical discretization, and consequently the implementation of the shallow water equations is typically an important intermediate step in model development.](#) A standard suite of reference solutions [to the shallow water equations](#) was suggested by [Williamson *et al.* \(1992\)](#), which [which continues to provide a useful means of](#) validation of new numerical schemes. The analytic nature of some of those solutions provide the obvious benefit that the dynamical fields are exactly knowable at all times. The solutions are limited, however, in that they do not possess the desirable nonlinearity and complexity of typical atmospheric flows. The need for a

more realistic benchmark flow prompted [Galewsky *et al.* \(2004\)](#) and [Polvani *et al.* \(2004\)](#) to seek a complex but numerically converged solution to the equations that might complement the analytic test cases of Williamson *et al.* The approach taken was that numerical resolution may be increased systematically until the point that the numerically generated flow evolution over a fixed time interval has converged to within a predefined tolerance, in the sense that further increases in resolution do not result in changes to the flow of greater magnitude than that tolerance, in some suitably defined measure. Because the solution thus obtained may be considered as an exact solution to the equations (to within the specified tolerance), it is thus independent of numerical scheme: any correct numerical implementation of the same equations must converge to the same solution.

To facilitate numerical convergence at moderate resolution, the benchmark solutions of [Galewsky *et al.* \(2004\)](#) and [Polvani *et al.* \(2004\)](#) included an explicit diffusion term in the equations of motion, of fixed strength, which limited the generation of small-scale motions to a fixed diffusive length scale, independent of resolution. In that case, numerical convergence was obtained relatively easily as soon as the numerical discretization was sufficiently fine to accurately represent the diffusive length scale. There are, however, two main drawbacks of that approach. The first is that the scales represented by these solutions are restricted to ones that are significantly greater than many important scales occurring in typical atmospheric motions, such as the formation of fronts or tropopause folds: the flow features of the Galewsky *et al.* and Polvani *et al.* solutions were limited to those that may be represented with a grid spacing of around 0.4° . A more stringent test of any numerical scheme lies in the accurate representation of much smaller-scale features, and these should therefore be present in a good benchmark solution.

The second drawback of the above solutions lies in the need for an explicit diffusion. For many numerical schemes, for example, finite volume or semi-Lagrangian

schemes (Lin and Rood 1997), diffusion of small-scale features is implicit in the scheme: the inherent diffusion due to interpolation errors is often sufficient to prevent the build-up of enstrophy at small scales and to stabilize the numerical evolution. To compute the benchmark solutions of Galewsky et al. and Polvani, et al., such numerical schemes would be required to add an additional explicit diffusion term to the underlying equations of motion, inconsistent with the underlying model philosophy, and complicating the validation of the desired operational scheme. Indeed, this difficulty has led various groups to compute the Galewsky et al. solution without introducing explicit diffusion (e.g. Chen et al. 2013; Salehipour et al. 2013; Ullrich et al. 2014, among many others). While this is convenient numerically and may give a crude indication that the numerical scheme is performing more or less correctly, it prevents the test case being used as a precise check of the numerical implementation and its accuracy. Thus, while the community clearly recognizes the importance for a refinement to the Galewsky et al. solution, so far none has been presented with a sufficient degree of rigour to enable accurate model validation (beyond being able to say that ones model is doing approximately the right thing).

In many commonly used numerical schemes, diffusion is linked to the grid scale and decreases as numerical resolution increases; the diffusive length scale thus also decreases, and the numerical solution approaches what is in essence a solution to the inviscid equations of motion. In this case, the extent to which numerical convergence is possible is limited by the nature of the solution. If the solution to the inviscid equations is such that a shock or infinite gradient in a particular field develops in a finite time (so that the solution is only valid in the appropriate weak sense) numerical convergence will not typically be achievable at any finite resolution. In situations of relevance to atmospheric flows, where gradients may be increasing exponentially in time, the issue of numerical convergence will now involve the specification of a fixed time interval over which convergence may be sought. Over this time

interval, solutions to the inviscid equations should be regular to the extent that all fields are representable by the numerical scheme at some achievable resolution.

In view of the above, it has become clear that an important addition to the Galewsky et al. (2004) and Polvani et al. (2004) benchmark solutions should consist of a numerical converged solution to the inviscid equations of motion in an appropriately defined time interval, over which sufficient nonlinearity and small-scale flow features develop, but over which solutions also remain sufficiently regular that a numerically converged inviscid solution may be obtained. Because of the tendency for rapid intensification of flow gradients in typical nonlinear flow fields, satisfying these two constraints turns out to be challenging, requiring computation at significantly higher resolutions than for the case of explicit diffusion. In the shallow water system, which will form the focus of this paper, sufficient resolutions may be reached with relative ease on current computers. The primitive equation case appears significantly more demanding, both on account of the need to increase simultaneously both horizontal and vertical resolution, and because small-scale development is considerably more active by virtue of the nature of the dynamics at the horizontal boundaries (e.g. Jukes 1995; Scott 2011).

The aim of the present short paper is thus to present a reference solution to the inviscid shallow water equations, which will be of potential use in the validation of the horizontal discretization component of new numerical schemes or implementations. It represents a small but nonetheless important advance on the viscous solution of Galewsky et al. (2004). The paper identifies a time interval over which the initial conditions (the same as those used in Galewsky et al. (2004)) generate a regular flow with features that may be captured at resolutions readily achievable on present-day computers. We present numerical converged solutions obtained using two separate numerical methods: a standard pseudo-spectral method (Hack and Jakob 1992; Rivier et al. 2002; Scott et al. 2004) and a

finite-volume method discretized on a cubed-sphere grid (Putman and Lin 2007; Harris and Lin 2013). We emphasize that the solution obtained is independent of numerical scheme and, furthermore, independent of any small-scale dissipation or filtering. Any numerical scheme solving the inviscid shallow-water equations should converge to this same solution, provided only that any artificial diffusion continually diminishes with increasing spatial resolution.

The remainder of this paper is organized as follows. In section two, we review the initial conditions; these are the same as those used in Galewsky *et al.* (2004) but are included here for completeness. In section three, we provide a brief description of the two numerical schemes used. In section four, we present solutions to the inviscid shallow water equations computed using the pseudo-spectral method, defining an appropriate time-interval over which convergence is obtained at the resolutions considered, and present various diagnostic quantities that may be used to quantify the convergence. In section five, we show the degree to which the solutions obtained are independent of the numerical scheme and present details of the rate of convergence in each case; these rates will in general vary from one numerical scheme to another.

2. Problem specification

We consider the equations for rotating shallow water on a sphere of radius $a = 6.37122 \times 10^6$ m:

$$\mathbf{u}_t + \mathbf{u} \cdot \nabla \mathbf{u} + f \hat{\mathbf{k}} \times \mathbf{u} = g \nabla h \quad (1a)$$

$$h_t + \nabla \cdot (\mathbf{u}h) = 0, \quad (1b)$$

where $\mathbf{u} = (u, v, 0)$ is the horizontal velocity, $\hat{\mathbf{k}}$ is the unit vector in the vertical, h is the fluid depth, $g = 9.80616 \text{ ms}^{-2}$ is gravity, and $f = 2\Omega \sin \phi$ is the Coriolis parameter, where $\Omega = 7.292 \times 10^{-5} \text{ s}^{-1}$ and ϕ is latitude.

Equations (1a,1b) are solved by integrating from specified initial conditions for \mathbf{u} and h . These comprise a barotropically unstable jet as defined in Galewsky *et al.* (2004), with zonally symmetric zonal velocity field $u =$

$u_0(\phi)$ given by:

$$u_0 = \frac{u_{\max}}{e_n} \exp [(\phi - \phi_0)(\phi - \phi_1)]^{-1} \quad \text{for } \phi_0 < \phi < \phi_1 \quad (2)$$

with $u = 0$ for $\phi \leq \phi_0$ and $\phi \geq \phi_1$. The functional form for u_0 has the advantage of being compact yet infinitely differentiable. The parameter values are $u_{\max} = 80 \text{ ms}^{-1}$, $\phi_0 = \pi/7$, $\phi_1 = \pi/2 - \phi_0$, and $e_n = \exp [-4(\phi_1 - \phi_0)^{-2}]$, for which the jet maximum is located at $\pi/4 = 45^\circ\text{N}$. The initial height field h_0 is defined from u_0 through gradient wind balance, that is, the v -component of (1a) for steady, axisymmetric flow, with the requirement that the global mean layer depth of the axisymmetric flow is $H = 10^4$ m. An important initial test of any numerical scheme is that this balanced and axisymmetric flow remain axisymmetric and steady in time. This is particularly important when considering numerical schemes that do not have an underlying zonal symmetry, such as those based on cubed-sphere or icosahedral grids.

To the axisymmetric flow we add a perturbation to the height field of the form:

$$h'(\lambda, \phi) = \hat{h} \cos \phi e^{-(\lambda/\alpha)^2} e^{-[(\phi - \phi_2)/\beta]^2} \quad (3)$$

where $-\pi < \lambda \leq \pi$ is longitude, $\phi_2 = \pi/4$, $\alpha = 1/3$, $\beta = 1/15$ and $\hat{h} = 120$ m. (This has the effect that the mean layer depth of the total initial condition modified very slightly to 10000.3 m.) The reader is referred to Figure 1 of Galewsky *et al.* (2004) for a graphical rendering of the initial basic state u_0 , h_0 and perturbation h' .

3. Numerical schemes

We use two independently developed numerical schemes to verify the accuracy of the solution. The first is the BOB pseudo-spectral scheme (Rivier *et al.* 2002), which solves the shallow water equations in vorticity-divergence form, with prognostic variables absolute vorticity $\zeta_a = 2\Omega \sin \phi + \mathbf{k} \cdot \nabla \times \mathbf{u}$, divergence $\delta = \nabla \cdot \mathbf{u}$, and height perturbation $\eta = h - H$. A small hyperdiffusive term $D =$

$-\nu\nabla^4\xi$ is included in the equation for each prognostic variable ξ , purely as a means to prevent enstrophy build-up at small scales. We note again the fundamental difference from Galewsky *et al.* (2004), where the coefficient ν was held fixed as resolution was increased. Here, in contrast, ν decreases with increasing resolution such that the diffusive timescale on the highest resolved wavenumber is constant across resolution. Thus, $\nu = \nu_*[a^2/N(N+1)]^2$ where N is the maximum total wavenumber at a particular resolution and ν_* is the diffusion rate at the smallest scale. It is fixed here at a value that is sufficient to control enstrophy over the time interval considered. We emphasize that the particular value of ν_* is unimportant and we purposefully omit giving its value here; in fact, the form of the diffusion operator ∇^{2n} may also be varied with essentially the same results. Neither do we consider here the question of how the diffusion should be chosen optimally. The important point is that the diffusion coefficient ν should tend to zero as resolution is increased. The solutions thus obtained may be considered to be solutions to the inviscid equations over the time interval over which they remain regular.

The second numerical scheme is the GFDL finite-volume cubed-sphere dynamical core (FV³), described in Putman and Lin (2007) and Harris and Lin (2013). FV³ is a finite-volume scheme on the equidistant gnomonic cubed-sphere grid Putman and Lin (2007) following the Lin and Rood (1997) shallow-water algorithm in the horizontal, which discretizes the vector-invariant (vorticity-kinetic energy form) shallow-water equations on the D grid using a forward-backward time integration, and computes the pressure gradient force through the algorithm of Lin (1997). Fluxes for mass, absolute vorticity, and kinetic energy are computed using a modification by Putman and Lin (2007) of the piecewise parabolic method (Colella and Woodward 1984). In the results presented below, the model was run in a configuration similar to that used in comprehensive climate simulations, in particular, including a monotonicity constraint and a standard scale-selective, fourth-order divergence damping. We emphasize again that

these details are unimportant. Indeed, the model was run separately with no monotonicity constraint and divergence damping at half the conventional rate; in both cases the model converges to the same solution presented below.

4. Inviscid solution

In this section we present results from the pseudospectral scheme only; we demonstrate in section 5 that the solutions obtained with the finite-volume scheme converge to the same flow.

Figure 1 shows snapshots of the evolution of the flow at 3 times, obtained from the numerical integration of (1–3) at the highest resolution considered. It illustrates eddy growth characteristic of barotropic instability, in which the spatially localized perturbation does not favour the growth of a particular wavenumber. The development is similar to that of Galewsky *et al.* (2004) but the higher effective Reynolds number here results in much more energetic generation of small-scale features, steep vorticity gradients and frontal regions. We take this to be our reference solution and it remains to establish over what time interval the solution can be considered to be numerically converged.

Figure 2 shows a magnification of the field at $t = 6$ days for a series of integrations at different numerical resolutions, from T85, corresponding to a grid of about 1.4° at the equator and comparable to the resolution used in many models of the CMIP5, to T2730, corresponding to a grid of about 0.044° at the equator (or about 5 km). Differences between successive panels decrease as resolution is increased. The last two panels are almost identical in terms of the position and shape of features such as the large cut-off low (a region of high potential vorticity) centred on 265°W , 30°N , or the undulation of the original jet. Even at these high resolutions, however, small differences between the two final panels may be detected in details such as the ridge of potential vorticity connecting the cut-off low to the jet undulation ($265\text{--}275^\circ\text{W}$, 20°N), or the degree to which potential vorticity gradients at the jet edge have been intensified (e.g., 292°W , 38°N).

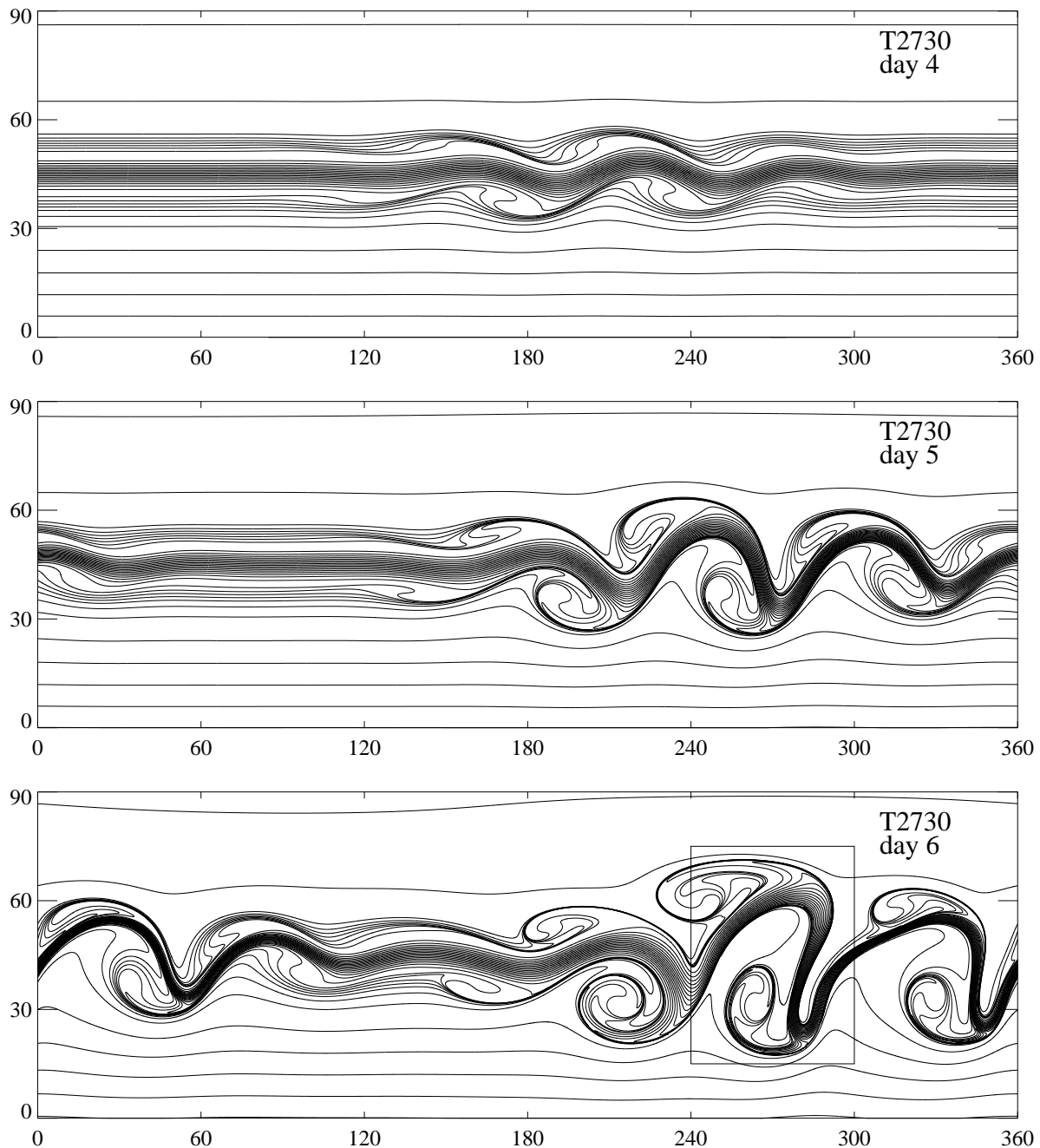


Figure 1. Snapshots of the flow evolution: potential vorticity, ζ_a/h , for the highest resolution case at $t = 4, 5, 6$ days. Contours are integer multiples of $0.2\Omega/H$.

Differences in the representation of the flow at different resolutions may be quantified by consideration of appropriate norms. The globally-averaged eddy kinetic energy, shown in Fig. 3a, illustrates the usual exponential growth of the perturbation from the zonal mean. Although it is a common measure of unstable development, it is a poor indicator of numerical convergence, being relatively insensitive to resolution, even for resolutions at which a casual inspection of the fields shown in Fig. 2 immediately reveals significant differences. Based on consideration of

the total eddy kinetic energy alone, one would conclude that the sequence of calculations had converged already at a resolution of T170; Fig. 2, on the other hand, shows that many small-scale features are poorly represented at this resolution. To a similar extent, the same can be said of the l_2 norm of the relative vorticity, Fig. 3b. The global averaging involved in the computation of these quantities obscures most of the differences clearly present in the fields themselves.

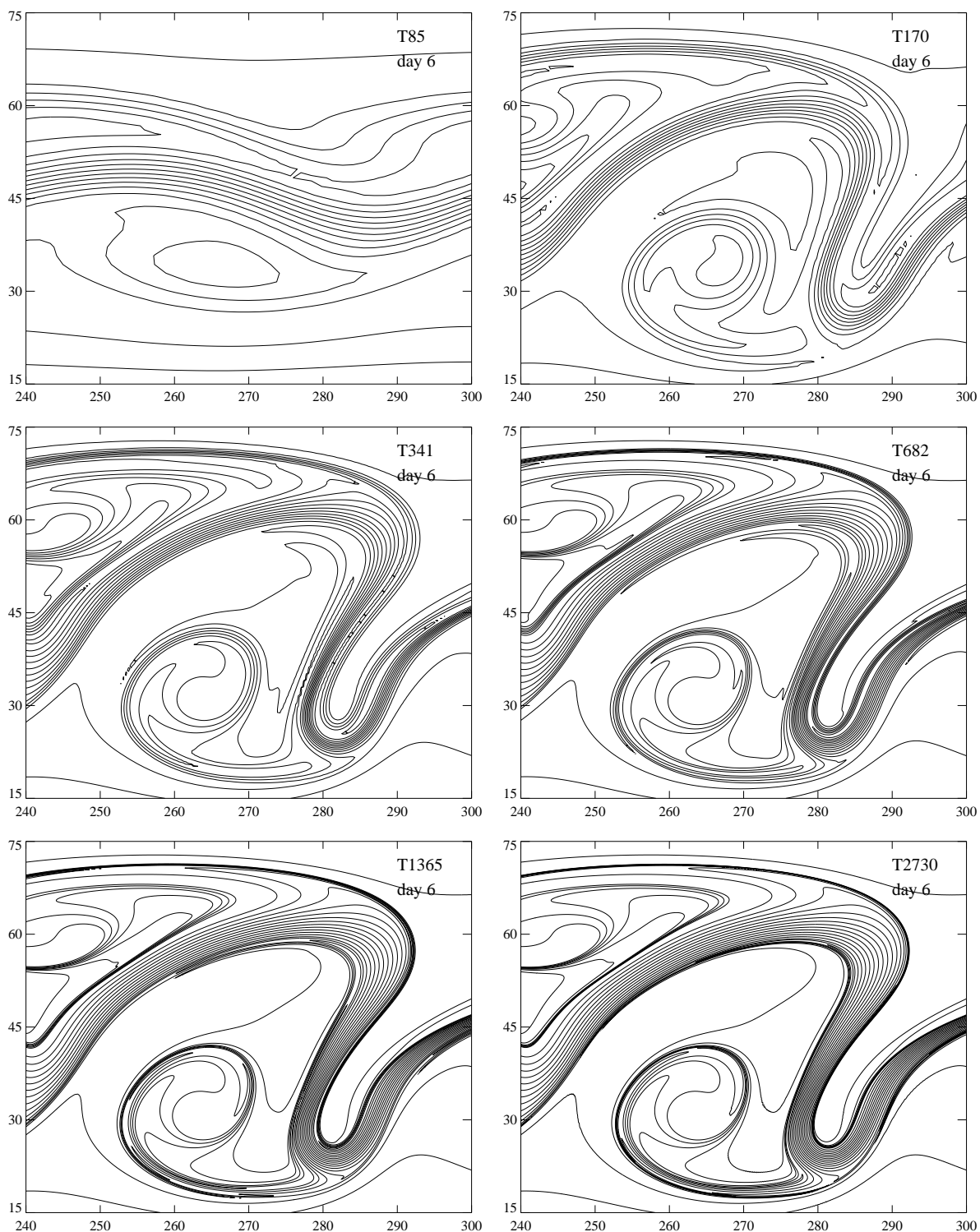


Figure 2. Potential vorticity at $t = 6$ days at resolutions increasing from T85 to T2730. The domain shown corresponds to the boxed region of Fig. 1c. Contours are integer multiples of $0.2\Omega/H$.

A more precise indicator of convergence is given by the l_∞ norms of quantities such as relative vorticity or potential vorticity, shown in Fig. 3c,d. The relative vorticity immediately reveals differences between even the two highest resolution integrations, T1365 and T2730, at $t = 6$ days. Extrapolation of the sequence of integrations

suggests that this quantity would be accurately represented at $t = 6$ perhaps only with a resolution of around T10000, which is impractical on present day computers. On the other hand, the values of $\|\zeta\|_\infty$ for the two highest resolutions remain indistinguishable on the plot up until around $t = 5$ days: the relative error at $t = 5$ between

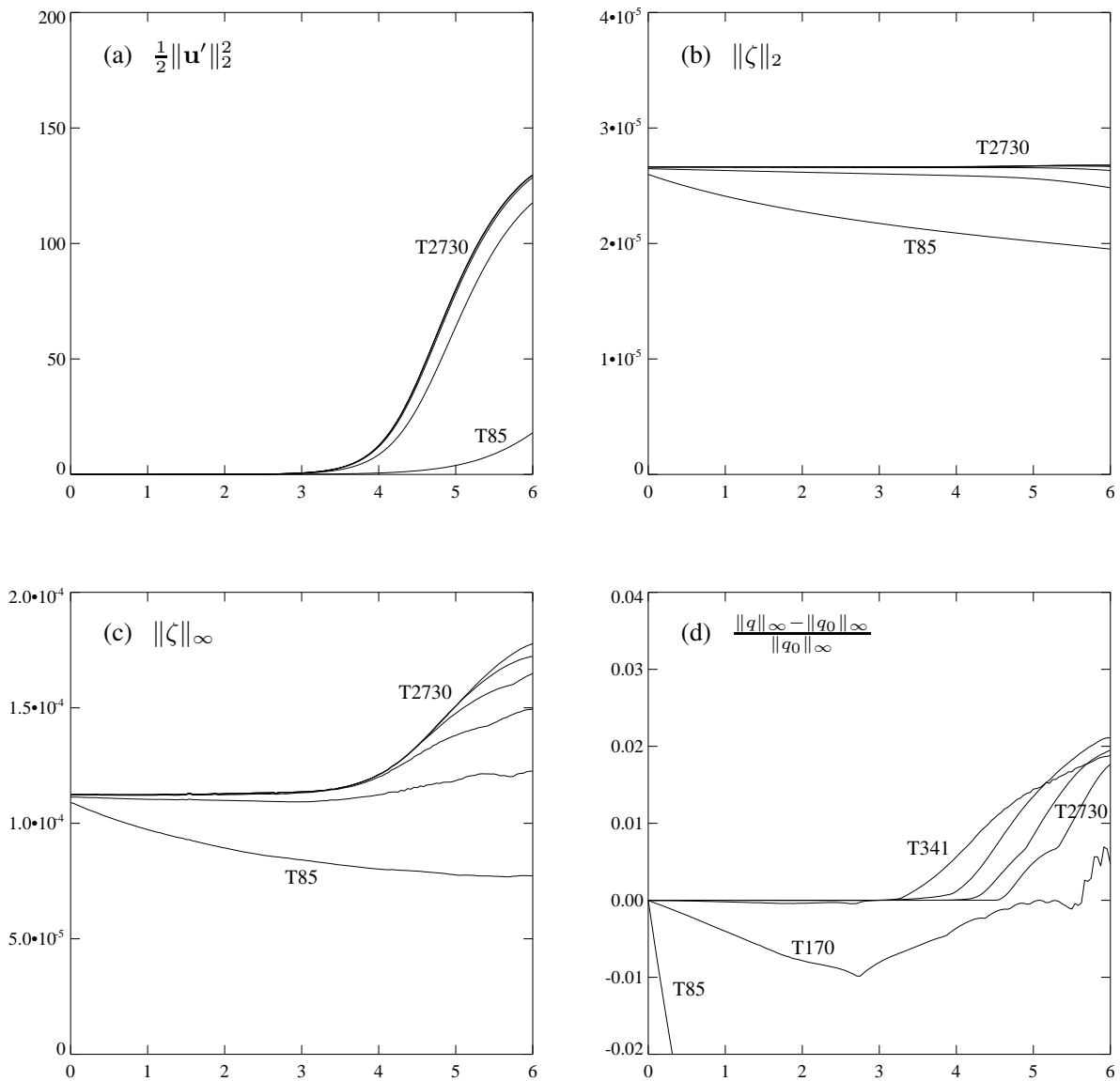


Figure 3. Diagnostic quantities as a function of time (in days): (a) globally-averaged eddy kinetic energy (units m^2s^{-2}); (b) rms relative vorticity (units s^{-1}); (c) maximum relative vorticity (units s^{-1}); (d) relative error of the maximum potential vorticity based on the initial potential vorticity, q_0 .

T1365 and T2730 (where the error is normalized by the highest resolution value) is approximately 0.0002. Based on the relative vorticity maximum, and an error tolerance of 0.0002 we could thus claim that the sequence has converged numerically at $t = 5$ days at a resolution of T2730. In fact, for practical purposes it turns out that a relative error tolerance of 0.005, or 0.5% is a good indication of convergence for this particular flow and this is the criterion that we adopt in the remainder of the paper. We note that other choices of time interval and error tolerance result in convergence at different resolutions. Our choice is motivated simply by the desire to have a test that may be implemented without the need for excessive

computational requirements, while retaining a reasonable level of complexity in the flow field.

Different quantities yield different convergence properties. Some, such as the maximum vorticity gradient are extremely sensitive and may indicate a relatively poor level of convergence, even at the resolutions considered here. A refinement of the vorticity maximum is to consider the potential vorticity maximum. (Potential vorticity has also been used as a convenient diagnostic in the evaluation of tracer schemes (Whitehead *et al.* 2015)). We may take advantage of the fact that potential vorticity is conserved exactly on fluid parcels in the inviscid system, and hence that we know *a priori* that $\|q\|_\infty = \text{constant}$ for the true

inviscid solution, even without the explicit calculation of such a solution. Departures of the numerically generated solution from the true inviscid solution, associated either with numerical errors or with processes associated with the small-scale dissipation, will in general be reflected in departures of $\|q\|_\infty$ from this constant initial value, $\|q_0\|_\infty$. Fig. 3d shows that $\|q\|_\infty$ is constant at early times, before significant enstrophy has cascaded to the smallest resolved scales. Departures from the inviscid solution appear at progressively later times as resolution is increased. At the highest resolution considered here, a departure from the inviscid value is visible in the plot as early as $t = 4.6$ days, just before the target time established above, although the relative error remains small, just below the 0.005 tolerance level at $t = 5$ days.

Our convergence criterion based on a relative error of $\|\zeta\|_\infty$ or $\|q\|_\infty$ below 0.005 is consistent with a visual comparison of the potential vorticity fields at the level of magnification used previously. Fig. 4 shows the same magnification of the same region as was considered Fig. 2 but for the two cases T1365 and T2730 at the time $t = 5$ days. The fields are very nearly identical aside from a single contour level that follows the extension of the potential vorticity ridge along the lower boundary of the jet core, a feature highly sensitive to numerical dissipation. Because the two-dimensional fields contain more information than the normed quantities, it is desirable that the criterion for convergence is based on both.

5. Robustness of the solution

Computation of the same solution with the alternative numerical scheme FV³ was carried out both to validate the pseudo-spectral solution, and to investigate the extent to which the rate of convergence depends on the particular scheme.

Figure 5 shows $\|\zeta\|_\infty$ and $\|q\|_\infty$ for the FV³ scheme for resolutions c80, corresponding to a grid resolution of 1.125° at the equator, to c2560, corresponding to a grid resolution of 0.035° . This range is comparable

to the range of resolutions used for the pseudospectral integrations. The relative vorticity indicates a similar rate of convergence of the FV³ scheme as the pseudospectral scheme. The relative errors compared with the c2560 solution at $t = 5$ days are 0.02 for c640 and 0.004 for c1280. In contrast, the potential vorticity maximum shows better behaviour to that of the pseudospectral case, remaining very nearly constant over the entire 6 day interval at resolutions c640 and higher. This may be expected from consideration of the way potential vorticity is treated numerically. In FV³ it is transported as a passive tracer with an advection scheme (Lin and Rood 1997) that prevents oscillatory errors. We note that in separate integrations of the same numerical scheme in which the monotonicity constraints are removed, the convergence of the potential vorticity maximum (not shown) looks similar to that found in the pseudospectral scheme, with departures from zero error appearing at progressively later times with increasing resolution, as in Fig. 3d. The results indicate that convergence characteristics, in the sense that one scheme may show better convergence in one norm than another, may vary from scheme to scheme, or even for a given scheme run with different means of numerical regularization. For example, the FV³ scheme without monotonicity constraint shows slightly better convergence in $\|\zeta\|_\infty$ but worse convergence in $\|q\|_\infty$ than the same scheme with monotonicity constraint included. While these details affect the rate of convergence, they do *not* affect the converged solution itself. Notwithstanding these subtleties, it is clear that at $t = 5$ days FV³ is converged at c2560 (with either choice of small-scale damping) according to the criterion put forward in the previous section.

Figure 6a shows the potential vorticity field $q(x, y)$ at $t = 5$ days at the highest FV³ resolution (thick dotted lines), plotted on top of same field at the highest pseudospectral resolution (thin red solid lines). The degree of agreement between the two calculations is exact in the visual comparison. This should not be surprising: both calculations are converged at this resolution to the unique solution

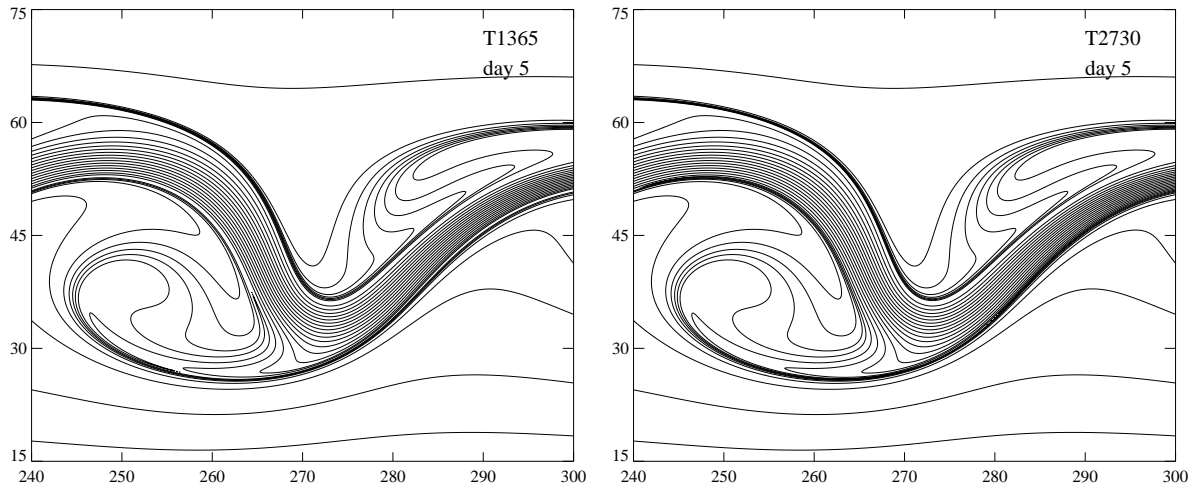


Figure 4. Potential vorticity at $t = 5$ days at resolutions T1365 and T2730. Contours are integer multiples of $0.2\Omega/H$.

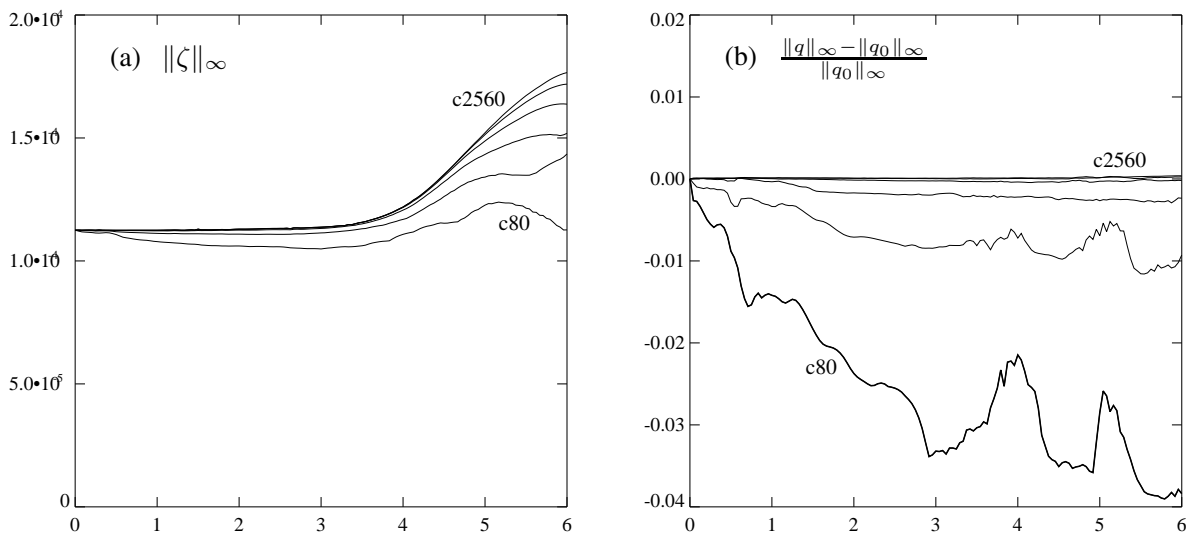


Figure 5. Diagnostic quantities as a function of time from the finite-volume integration; (a) maximum relative vorticity; (b) relative error of the maximum potential vorticity.

of the equations with the prescribed initial condition. Discrepancies between the two solutions would imply either that one or other numerical scheme had not converged, or else a failure in one of the numerical schemes to converge to the correct solution.

We noted previously that the solutions obtained with each scheme are not fully converged at the later time of $t = 6$ days, in the sense that the two highest resolution fields of each numerical scheme (T1365 and T2730 for pseudospectral, c1280 and c2560 for FV³) are not identical. Nonetheless, it is interesting to observe that at the very highest resolution the two schemes agree with each other to a remarkable extent, as shown in Figure 6b. While we are unable to compare these fields to ones at an even higher

resolution, the fact that the two independent numerical schemes agree to such a close extent is highly suggestive that the flow given in the figure is an accurate representation of the true solution at $t = 6$ days. [The same conclusion was obtained from the results of FV³ with no monotonicity constraint and weaker divergence damping.](#)

Finally, Fig. 7 shows the pointwise relative errors at different resolutions of the solutions calculated with both schemes, where the “true” solution is taken to be the highest resolution solution in each case. At each resolution, the error is computed by interpolating the low resolution velocity fields onto the high resolution grid, taking the difference between the low and high resolution velocity fields, and then computing the eddy kinetic energy of this

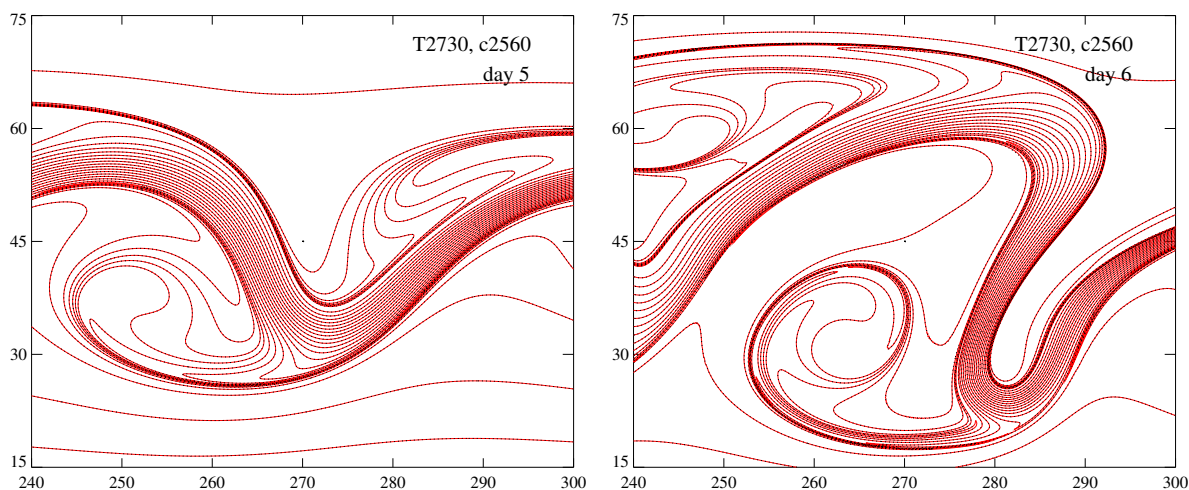


Figure 6. Potential vorticity from the finite-volume integration at (a) $t = 5$ days and (b) $t = 6$ days at resolutions c2160 (dotted) superposed on the same field from the pseudospectral integration at resolution T2730 (thin red lines).

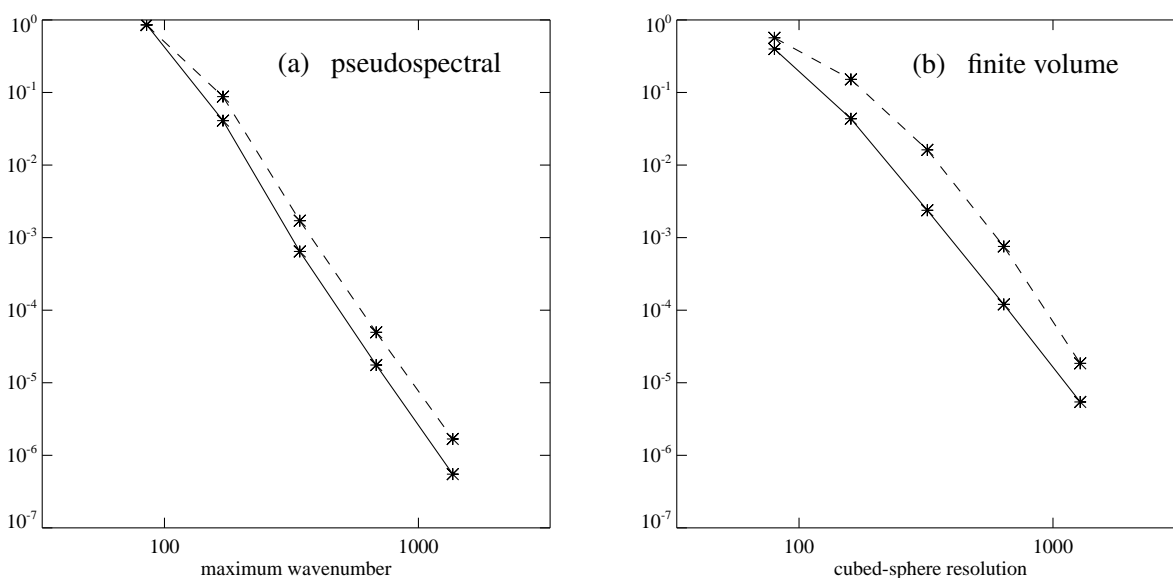


Figure 7. Eddy kinetic energy: relative error from highest resolution solution at $t = 5$ days (solid) and $t = 6$ days (dotted): (a) pseudo-spectral integration, (b) finite-volume integration.

difference. Errors are computed in this way both at $t = 5$ days (solid) and $t = 6$ days (dashed), with larger errors occurring at the later time as expected. Both pseudospectral and FV³ schemes show algebraic decrease in error with increasing resolution, with slightly faster decrease for the pseudospectral scheme. FV³ has less error at the lowest c80 resolution because it has a well-developed breaking wave on days 5 and 6, as opposed to the pseudospectral solution at T85 (see Fig. 2); it has higher errors at the highest resolutions, mostly likely due to edge and corner effects in the cubed-sphere grid. Again, the relative rates of convergence of the two schemes will depend on the particular norms used to quantify them. However, as we

are less interested in the relative merits of one numerical scheme over another than in simply ensuring that the solutions converge at some reasonable resolution, we do not analyze these differences further.

6. Summary

In this paper we have presented a numerically converged solution of the rotating shallow water equations (1a,1b) and initial conditions (2,3) in the limit of vanishing viscosity. The solution is established over a time interval of 5 days, by which time small-scale features representative of atmospheric flows have developed. The intention is that the

solution will be a useful tool against which new numerical schemes may be validated.

The first step in the validation procedure is the integration of the equations from the initial conditions to $t = 5$ days at progressively higher resolutions, and decreasing dissipation, whether explicit or implicit to the numerical scheme, until such a point that the sequence of solutions thus generated has converged. Again, we emphasize that the details of the numerical or explicit diffusion are unimportant, provided only that they yield a stable solution. Here, the sequence of solutions may be considered converged when the l_∞ norm of the relative vorticity gives a relative error, based on the difference between the two highest resolutions solutions, of less than 0.005. As an alternative or additional measure, it may be required that the l_∞ norm of the potential vorticity also gives a relative error less than 0.005, where here the relative error is based on the difference between the highest resolution solution and the maximum potential vorticity at $t = 0$. Because the norms are single value quantities, it is further recommended that the two-dimensional potential vorticity fields of the two highest resolution solutions are compared at a magnification similar to that of Figure 4. Differences in the positions of the contours should be minimal. It should be borne in mind that the resolution at which convergence occurs will in general vary from scheme to scheme and may differ from the ones reported here.

Once it has been established that the sequence of solutions has converged by the above criteria, the highest resolution solution should be compared with the field shown in Figure 6. * The solutions should match to the level of agreement shown in that figure; in particular, there should be no discernible difference in the contour positions at this level of magnification. As a further quantitative measure we

provide the following values at $t = 5$ days:

$$\begin{aligned} \text{eddy kinetic energy :} & \quad 81.14 \pm 0.05 \text{ m}^2 \text{ s}^{-2} \\ \|\zeta\|_2 : & \quad 2.67251 \pm 0.0006 \times 10^{-5} \text{ s}^{-1} \\ \|\zeta\|_\infty : & \quad 1.51175 \pm 0.0003 \times 10^{-4} \text{ s}^{-1} \\ \|q\|_\infty : & \quad 2.42909 \pm 0.01 \times 10^{-8} \text{ m}^{-1} \text{ s}^{-1} \end{aligned}$$

where the error bounds have been taken (conservatively) from the difference between the values obtained at the two highest resolution pseudospectral solutions.

Finally, pointwise relative errors may be computed to indicate the rate of convergence of the particular numerical scheme and may be compared against those of the pseudospectral and FV³ schemes shown in Fig. 7. We emphasize that rates of convergence will in general vary from one scheme to another, and, moreover, may depend on the particular norm used to define convergence.

We close by providing a brief indication of the magnitude of errors that may be expected from errors in the numerical implementation of the governing equations (1a,1b). For simplicity we consider the effect of errors introduced in the physical parameters Ω , a , and g . Of these it was found that the solution was most sensitive to errors in Ω and a . As an example, when the value of a was set erroneously to 6.39×10^6 m, an error of approximately 0.25%, the converged solution changed by an amount shown in Fig. 8, where the correct solution is contoured in thin red lines and the wrong solution is contoured in black dotted lines. The values of the quantities in the above list are: eddy kinetic energy, $79.9 \text{ m}^2 \text{ s}^{-2}$; $\|\zeta\|_2$, $2.66 \times 10^{-5} \text{ s}^{-1}$; $\|\zeta\|_\infty$, $1.50 \times 10^{-4} \text{ s}^{-1}$; $\|q\|_\infty$, $2.44 \times 10^{-8} \text{ m}^{-1} \text{ s}^{-1}$; all of which lie outside the error bounds indicated. Consideration of either the field shown in Fig. 8 or the normed quantities listed here would thus correctly lead to the rejection of this solution and point to an error in the numerical implementation.

References

- Chen C, Bin J, Xiao F, Li X, Shen X. 2013. A global shallow-water model on an icosahedral-hexagonal grid by a multi-moment

*To facilitate this comparison we have included datasets of potential vorticity at days 5 and 6 as supplementary online material.

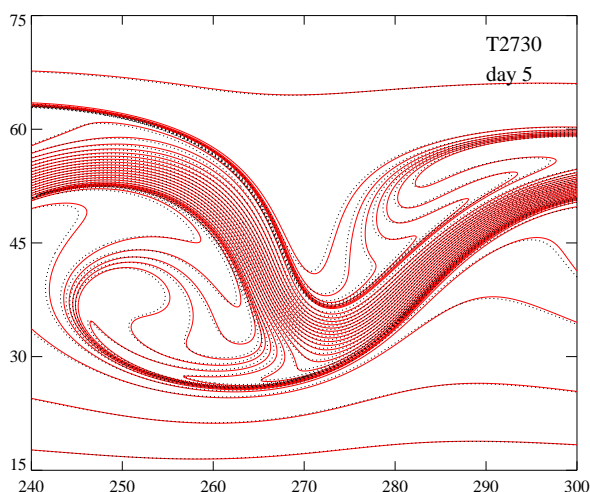


Figure 8. Potential vorticity at $t = 5$ days of the correct solution (thin red lines) and a solution obtained from an integration with α defined erroneously as 6.39×10^6 m (black dotted lines). Both solutions were obtained with the pseudospectral scheme at T2730.

- constrained finite-volume scheme. *Q. J. R. Meteorol. Soc.* **140**: 639–650.
- Colella P, Woodward PR. 1984. The piecewise parabolic method (PPM) for gas-dynamical simulations. *J. Comput. Phys.* **54**: 174–201.
- Galewsky J, Scott RK, Polvani LM. 2004. An initial-value problem for testing numerical models of the global shallow water equations. *Tellus A* **56**: 429–440.
- Hack JJ, Jakob R. 1992. Description of a global shallow water model based on the spectral transform method. *NCAR Technical Note* : 41ppNCAR/TN-232+STR.
- Harris LM, Lin SJ. 2013. A two-way nested global-regional dynamical core on the cubed-sphere grid. *Monthly Weather Review* **141**: 283–306.
- Juckes M. 1995. Instability of surface and upper-tropospheric shear lines. *J. Atmos. Sci.* **52**: 3247–3262.
- Lin SJ. 1997. A finite-volume integration method for computing pressure gradient force in general vertical coordinates. *Q. J. Roy. Meteor. Soc.* **123**: 1749–1762.
- Lin SJ, Rood R. 1997. An explicit flux-form semi-Lagrangian shallow-water model on the sphere. *Q. J. Roy. Meteor. Soc.* **123**: 2477–2498.
- Polvani LM, Scott RK, Thomas SJ. 2004. Numerically converged solutions of the global primitive equations for testing the dynamical core of atmospheric GCMs. *Mon. Weather Rev.* **132**: 2539–2552.
- Putman WM, Lin SJ. 2007. Finite-volume transport on various cubed-sphere grids. *J. Comp. Phys.* **227**: 55–78.
- Rivier L, Loft R, Polvani LM. 2002. An efficient spectral dynamical core for distributed memory computers. *Mon. Weather Rev.* **130**: 1384–1390.

- Salehipour H, Stuhne GR, Peltier WR. 2013. A higher order discontinuous galerkin, global shallow water model: Global ocean tides and aquaplanet benchmarks. *Ocean Mod.* **107**: 69–93.
- Scott RK. 2011. A scenario for finite-time singularity in the quasigeostrophic equations. *J. Fluid Mech.* **687**: 492–502.
- Scott RK, Rivier L, Loft R, Polvani LM. 2004. BOB: Model implementation and users guide. *NCAR Technical Note* : 30ppNCAR/TN-456+IA.
- Ullrich PA, Lauritzen PH, Jablonowski C. 2014. A high-order fully explicit flux-form semi-lagrangian shallow water model. *Int. J. Num. Meth. Fluids* **75**: 103–133.
- Whitehead JP, Jablonowski C, Kent J, Rood RB. 2015. Potential vorticity: Measuring consistency between GCM dynamical cores and tracer advection schemes. *Q. J. Roy. Met. Soc.* **141**: 739–751.
- Williamson DL, Drake JB, Hack JJ, Jakob R, Swartztrauber PN. 1992. A standard test set for numerical approximations to the shallow water equations in spherical geometry. *J. Comp. Phys.* **102**: 211–224.